DRAFT VERSION MARCH 6, 2014.
Preprint typeset using LaTeX style emulateapj v. 5/2/11

arXiv:1403.1230v1 [astro-ph.HE] 5 Mar 2014

MAGNETOROTATIONAL CORE-COLLAPSE SUPERNOVAE IN THREE DIMENSIONS

PHILIPP MÖSTA[1], SHERWOOD RICHERS[1], CHRISTIAN D. OTT[1,2,+], ROLAND HAAS[1], ANTHONY L. PIRO[1], KRISTEN BOYDSTUN[1], ERNAZAR ABDIKAMALOV[1], CHRISTIAN REISSWIG[1,++], AND ERIK SCHNETTER[3,4,5]

Draft version March 6, 2014.

ABSTRACT

We present results of new three-dimensional (3D) general-relativistic magnetohydrodynamic simulations of rapidly rotating strongly magnetized core collapse. These simulations are the first of their kind and include a microphysical finite-temperature equation of state and a leakage scheme that captures the overall energetics and lepton number exchange due to postbounce neutrino emission. Our results show that the 3D dynamics of magnetorotational core-collapse supernovae are fundamentally different from what was anticipated on the basis of previous simulations in axisymmetry (2D). A strong bipolar jet that develops in a simulation constrained to 2D is crippled by a spiral instability and fizzles in full 3D. While multiple (magneto-)hydrodynamic instabilities may be present, our analysis suggests that the jet is disrupted by an $m = 1$ kink instability of the ultra-strong toroidal field near the rotation axis. Instead of an axially symmetric jet, a completely new, previously unreported flow structure develops. Highly magnetized spiral plasma funnels expelled from the core push out the shock in polar regions, creating wide secularly expanding lobes. We observe no runaway explosion by the end of the full 3D simulation at 185 ms after bounce. At this time, the lobes have reached maximum radii of $\sim$900 km.

Subject headings: gamma-ray burst: general – instabilities – magnetohydrodynamics – neutrinos – supernovae: general

1. INTRODUCTION

Stellar collapse liberates gravitational energy of order $10^{53}\,\mathrm{erg\,s^{-1}}$ (100 B). Most (99%) of that energy is emitted in neutrinos, and the remainder ($\lesssim 1$ B) powers a core-collapse supernova (CCSN) explosion. However, a small fraction of CCSNe are hyper-energetic (~ 10 B) and involve relativistic outflows (e.g., Soderberg et al. 2006; Drout et al. 2011). These *hypernovae* come from stripped-envelope progenitors and are classified as Type Ic-bl (H/He deficient, broad spectral lines). Importantly, all SNe connected with long gamma-ray bursts (GRB) are of Type Ic-bl (Modjaz 2011; Hjorth & Bloom 2011).

Typical $\mathcal{O}(1)$B SNe may be driven by the *neutrino mechanism* (Bethe & Wilson 1985), in which neutrinos emitted from the collapsed core deposit energy behind the stalled shock, eventually driving it outward (e.g., Müller et al. 2012; Bruenn et al. 2013). However, the neutrino mechanism appears to lack the efficiency needed to drive hyperenergetic explosions. One possible alternative is the *magnetorotational* mechanism (e.g. Bisnovatyi-Kogan 1970; LeBlanc & Wilson 1970; Meier et al. 1976; Wheeler et al. 2002). In its canonical form, rapid rotation of the collapsed core (Period $\mathcal{O}(1)$ ms, spin energy $\mathcal{O}(10)$ B) and magnetar-strength magnetic field with a dominant toroidal component drive a strong bipolar jet-like explosion that could result in a hypernova (Burrows et al. 2007).

The magnetorotational mechanism requires rapid precollapse rotation ($P_0 \lesssim 4$ s; Ott et al. 2006; Burrows et al. 2007) and an efficient process to rapidly amplify the likely weak seed magnetic field of the progenitor. The *magnetorotational instability* (MRI, Balbus & Hawley 1991; Akiyama et al. 2003; Obergaulinger et al. 2009) is one possibility. The MRI operates on the free energy of differential rotation and, in combination with dynamo action, has been hypothesized to provide the necessary global field strength on an essentially dynamical timescale (Akiyama et al. 2003; Thompson et al. 2005). The wavelength of the fastest growing MRI mode in a postbounce CCSN core is much smaller than what can currently be resolved in global multi-dimensional CCSN simulations. Under the assumption that MRI and dynamo operate as envisioned, a common approach is to start with a likely unphysically strong precollapse field of $10^{12}-10^{13}$ G. During collapse and the early postbounce evolution, this field is amplified by flux compression and rotational winding to dynamically important field strength of $B_{\rm tor} \gtrsim 10^{15}-10^{16}$ G (Burrows et al. 2007). In this way, a number of recent two-dimensional (2D) magnetohydrodynamic (MHD) simulations have found robust and strong jet-driven explosions (e.g., Shibata et al. 2006; Burrows et al. 2007; Takiwaki & Kotake 2011). Only a handful of 3D studies have been carried out with varying degrees of microphysical realism (Mikami et al. 2008; Kuroda & Umeda 2010; Scheidegger et al. 2010; Winteler et al. 2012) and none have compared 2D and 3D dynamics directly.

In this *Letter*, we present new full 3D dynamical-spacetime general-relativistic MHD (GRMHD) simulations of rapidly rotating magnetized CCSNe. These are the first to employ a microphysical finite-temperature equation of state, a realistic progenitor model, and an approximate neutrino treatment for collapse and postbounce evolution. We carry out simulations in full unconstrained 3D and compare with simulations starting from identical initial conditions, but constrained to 2D. Our results for a model with initial poloidal B-field of 10^{12} G indicate that 2D and 3D magnetorotational CCSNe are fundamentally different. In 2D, a strong jet-driven explosion obtains, while in unconstrained 3D, the developing jet is destroyed by nonaxisymmetric dynamics, caused most likely by

[1] TAPIR, Mailcode 350-17, California Institute of Technology, Pasadena, CA 91125, USA, pmoesta@tapir.caltech.edu
[2] Kavli Institute for the Physics and Mathematics of the Universe (Kavli IPMU WPI), The University of Tokyo, Kashiwa, Japan
[3] Perimeter Institute for Theoretical Physics, Waterloo, ON, Canada.
[4] Department of Physics, University of Guelph, Guelph, ON, Canada.
[5] Center for Computation & Technology, Louisiana State University, Baton Rouge, USA.
[+] Alfred P. Sloan Research Fellow
[++] NASA Einstein Fellow

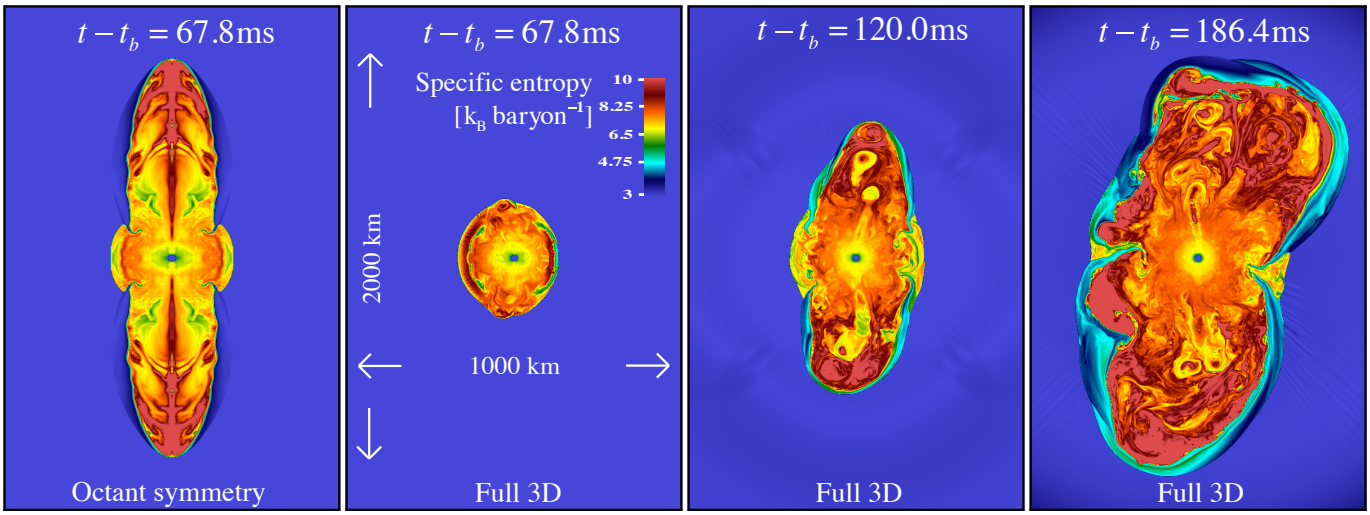

Figure 1. Meridional slices ($x-z$ plane; z being the vertical) of the specific entropy at various postbounce times. The "2D" (octant 3D) simulation (leftmost panel) shows a clear bipolar jet, while in the full 3D simulation (3 panels to the right) the initial jet fails and the subsequent evolution results in large-scale asymmetric lobes.

an $m = 1$ MHD kink instability. The subsequent CCSN evolution leads to two large asymmetric shocked lobes at high latitudes. Highly-magnetized tubes tangle, twist, and drive the global shock front steadily, but not dynamically outward. A runaway explosion does not occur during the $\sim$185 ms of postbounce time covered by our full 3D simulation.

2. METHODS AND SETUP

We employ ideal GRMHD with adaptive mesh refinement (AMR) and spacetime evolution provided by the open-source `EinsteinToolkit` (Mösta et al. 2014; Löffler et al. 2012). GRMHD is implemented in a finite-volume fashion with WENO5 reconstruction (Reisswig et al. 2013; Tchekhovskoy et al. 2007) and the HLLE Riemann solver (Einfeldt 1988) and constrained transport (Tóth 2000) for maintaining div$B = 0$. We employ the $K_0 = 220$ MeV variant of the equation of state of Lattimer & Swesty (1991) and the neutrino leakage/heating approximations described in O'Connor & Ott (2010) and Ott et al. (2012). At the precollapse stage, we cover the inner $\sim$5700 km of the star with four AMR levels and add five more during collapse. After bounce, the protoneutron star is covered with a resolution of $\sim$370 m and AMR is set up to always cover the shocked region with at least 1.48 km linear resolution.

We draw the 25-$M_\odot$ (at zero-age-main-sequence) presupernova model E25 from Heger et al. (2000) and set up axisymmetric precollapse rotation using the rotation law of Takiwaki & Kotake (2011) (see their Eq. 1) with an initial central angular velocity of 2.8 rad s^{-1}. The fall-off in cylindrical radius and vertical position is controlled by parameters $x_0 = 500$ km and $z_0 = 2000$ km, respectively. We set up the initial magnetic field by a vector potential of the form $A_r = A_\theta = 0; A_\phi = B_0(r_0^3)(r^3 + r_0^3)^{-1} r \sin\theta$, where B_0 controls the strength of the field. In this way we obtain a modified dipolar field structure that stays nearly uniform in strength within radius r_0 and falls off like a dipole at larger radii. We set $B_0 = 10^{12}$ G and choose $r_0 = 1000$ km to match the initial conditions of model B12X5β0.1 of the 2D study of Takiwaki & Kotake (2011), in which a jet-driven explosion is launched $\sim$20 ms after bounce.

We perform simulations both in full, unconstrained 3D and in octant symmetry 3D (90-degree rotational symmetry in the $x-y$ plane and reflection symmetry across the $x-y$ plane) with otherwise identical setups. Octant symmetry suppresses most nonaxisymmetric dynamics, since it allows only modes with azimuthal numbers that are multiples of $m = 4$. In order to study the impact of potential low-mode nonaxisymmetric dynamics on jet formation, we add a 1% $m = 1$ perturbation to the full 3D run. Focusing on a potential instability of the strong toroidal field near the spin axis, we apply this perturbation to the velocity field within a cylindrical radius of 15 km and outside the protoneutron star, 30 km $\leq |z| \leq$ 75 km, at 5 ms after bounce.

3. RESULTS

Collapse and the very early postbounce evolution proceed identically in octant symmetry and full 3D. At bounce, $\sim$350 ms after the onset of collapse, the poloidal and toroidal B-field components reach $B_{\rm pol}, B_{\rm tor} \sim 10^{15}$ G. The hydrodynamic shock launched at bounce, still approximately spherical, stalls after $\sim$10 ms at a radius of $\sim$110 km. Rotational winding, operating on the extreme differential rotation in the region between inner core and shock, amplifies the toroidal component to 10^{16} G near the rotation axis within $\sim$20 ms of bounce. At this time, the strong polar magnetic pressure gradient, in combination with hoop stresses excerted by the toroidal field, launches a bipolar outflow. As depicted by the leftmost panel of Fig. 1, a jet develops and reaches $\sim$800 km after $\sim$70 ms in the octant-symmetry run. The expansion speed at that point is mildly relativistic ($v_r \simeq 0.1 - 0.15\,c$). This is consistent with the 2D findings of Takiwaki & Kotake (2011).

The full 3D run begins to diverge from its more symmetric counterpart around $\sim$15 ms after bounce. A nonaxisymmetric spiral ($m = 1$) deformation develops near the rotation axis. It distorts and bends the initially nearly axisymmetrically developing jet, keeping it from breaking out of the stalled shock. The nearly prompt magnetorotational explosion of the octant-symmetry run *fails* in full 3D. The subsequent 3D evolution is fundamentally different from 2D, as evidenced by the three panels of Fig. 1 depicting meridional specific entropy slices at different times in the full 3D run. Until 80 ms, the shock remains stalled and nearly spherical. The $m = 1$ dynamics per-

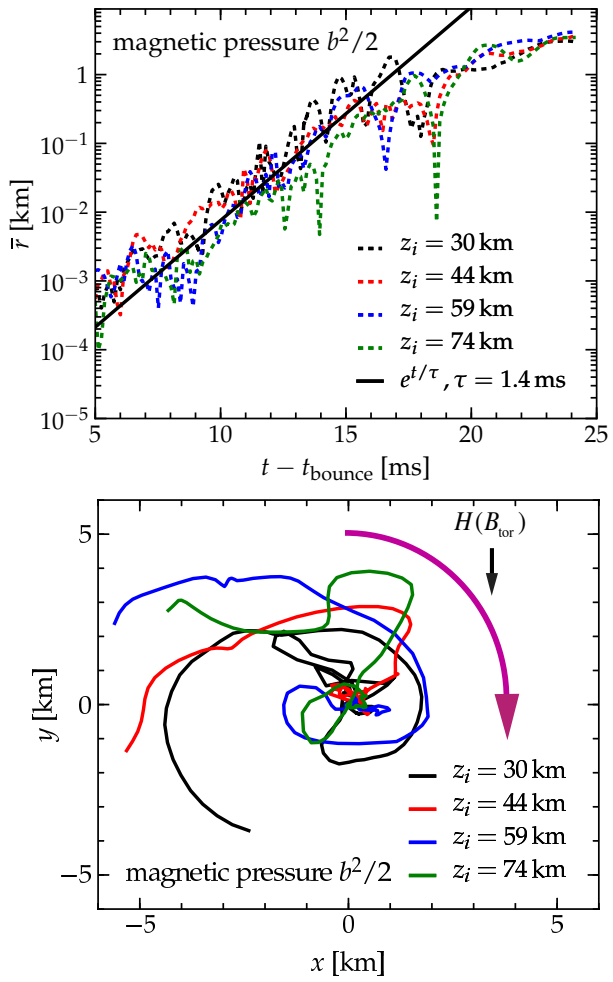

Figure 2. Top panel: Barycenter displacement $\bar{r}$ of b^2 in $x-y$ planes at different heights z_i. To minimize the influence of material that does not belong to the unstable jet, we include only cells inside a radius of 15 km. We observe exponential growth of the displacement in the early postbounce evolution until saturation at $t - t_b \sim 20$ ms. The growth rate $\tau_{fgm,sim} \approx 1.4$ ms is consistent with estimates for the MHD kink instability (see Section 3.1). **Bottom panel**: Tracks of the barycenter in the $x-y$ plane at different z_i. They are plotted for the interval shown in the top panel. The tracks trace the spiral nature of the displacement. Note that, as required for the perturbation to be unstable (Begelman 1998), the helicity of the displacement motion (counterclockwise in the $x-y$ plane) is opposite to the helicity of the toroidal magnetic field $H(B_{\rm tor})$ (clockwise in the $x-y$ plane), indicated by the magenta arrow.

vade the entire postshock region and cause a spiral-sloshing of the shock front that is reminiscent of the standing-accretion shock instability in rotating 3D CCSNe (cf. Kuroda et al. 2013). Later, highly-magnetized ($\beta = P_{\rm gas}/P_{\rm mag} \ll 1$) funnels of high-entropy material protrude from polar regions of the core and secularly push out the shock into two dramatic tilted lobes. At the end of our simulation ($\sim$185 ms after bounce) the lobes fill polar cones of $\sim 90^\circ$ and are only gradually expanding as low-β material is pushed out from below. Accreting material is deflected by these lobes and pushed towards the equator where it accretes through the remainder of the initial nearly spherical shock.

3.1. *Nonaxisymmetric Instability and Jet Formation*

The results discussed in the above suggest that the full 3D run is subject to a spiral instability that grows from $\sim 1\%$ $m = 1$ seeds in the velocity field to non-linear scale within the first $\sim$20 ms after bounce. This instability quenches the jet. Figure 2 depicts the linear growth and non-linear saturation of the spiral instability at various locations along the spin axis outside the protoneutron star.

In the rotating CCSN context, rotational shear instabilities in the protoneutron star (e.g., Ott et al. 2007) and a spiral standing accretion shock instability (SASI; e.g., Kuroda et al. 2013) have been discussed to potentially arise already at early postbounce times. It is unlikely that either of these is excited in our simulations, since we choose to perturb a radially and vertically narrow region along the spin axis outside of the protoneutron star and far from the shock, within the region of the highest toroidal magnetic field strength. A spiral MHD instability may thus be the driving agent behind the strong asymmetry in our simulation.

One possible such instability is the screw-pinch kink instability that has been studied in jets from active galactic nuclei (e.g., Begelman 1998; Mignone et al. 2010; McKinney & Blandford 2009). The B-field near the spin axis in our simulation can be roughly approximated by a screw-pinch field configuration. This consists of a non-rotating plasma cylinder and a magnetic field of the form

$$\vec{B} = B_{\rm tor}(r)\hat{\phi} + B_z\hat{z}\,, \qquad (1)$$

where $\hat{z}$ is along the rotation axis, $\hat{\phi}$ is in the toroidal direction, B_z is a constant vertical component of the B-field, and $B_{\rm tor}(r)$ is the radially-varying toroidal component of the B-field. We can express perturbations to the jet in the form of fluid displacements as a sum of basis elements of the form $\vec{\xi}_{km} \propto e^{i(kz+m\phi-\omega t)}$, where m is an integer, k is the vertical wave number, and ω is the oscillation frequency of the mode. The Kruskal-Shafranov stability criterion states that a plasma cylinder confined to a finite radius a (as in a tokamak) is unstable to kink ($m = \pm 1$) modes if $B_{\rm tor}/B_z > 2\pi a/L$, where L is the length of the cylinder and the sign of m is such that the mode's helicity is opposite to the field helix (Shafranov 1956; Kruskal & Tuck 1958). Unconfined screw-pinch structures with $B_{\rm tor} \gg B_z$ have been shown to be violently unstable to $m = 1$ modes at short vertical wavelengths ($kr \gg 1$) when $d\ln B_{\rm tor}/d\ln r > -1/2$ and the plasma parameter is sufficiently large ($\beta > 2/3\gamma$ where γ is the local adiabatic index). Under these conditions (which are only approximately met in our simulation), the fastest growing unstable mode (fgm) is amplified on a timescale comparable to the Alfvén travel time around a toroidal loop (Begelman 1998). The expected $m = 1$ growth timescale and vertical wavelength in the most unstable regions of the jet at $\sim$10 – 15 ms after bounce are

$$\tau_{\rm fgm} \approx \frac{4a\sqrt{\pi\rho}}{B_{\rm tor}} \approx 1\,{\rm ms}\,, \qquad \lambda_{\rm fgm} \approx \frac{4\pi a B_z}{B_{\rm tor}} \approx 5\,{\rm km}\,,$$

where a is the radius of the most unstable region. The growth time is much shorter than the time it would take for the jet to propagate through the shocked region.

The effect of the kink instability can be most clearly seen in a displacement of the jet barycenter away from the rotation axis of the core. We measure the displacement of the jet in our full 3D run by computing the barycenter displacement (planar "center-of-mass" displacement; Mignone et al. 2010) of the co-moving magnetic field strength b^2 (see, e.g., Mösta et al. 2014) in xy-slices at different heights z_i along the rotation axis (Fig. 2). b^2 probes the MHD effects in our simulations most directly, but other variable choices, e.g. the specific entropy s, exhibit similar behavior as flux freezing couples fluid proper-

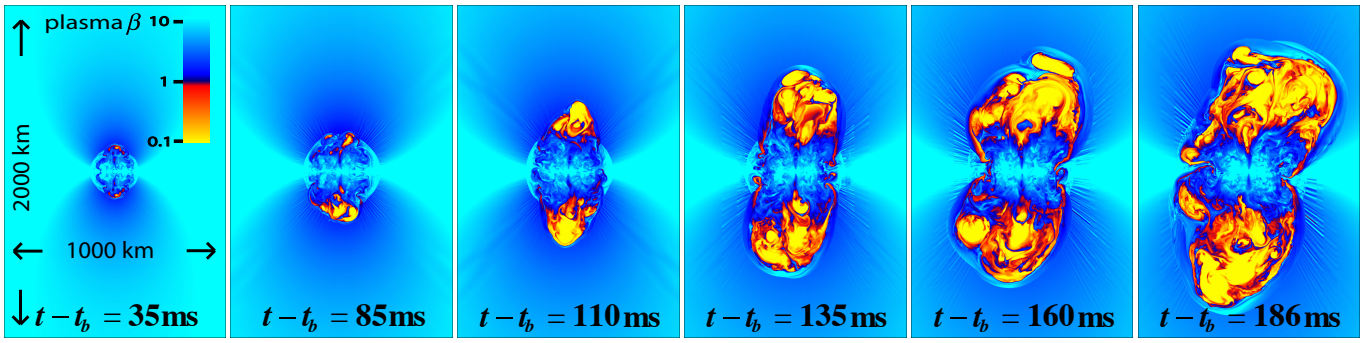

Figure 3. Meridional slices ($x-z$ plane) of the plasma $\beta = P_{\rm gas}/P_{\rm mag}$ at different postbounce times. The z-axis of the frames is the vertical and the rotation axis, x is the horizontal. The colormap is saturated at a minimum $\beta = 0.01$ and a maximum $\beta = 10$. Regions of $\beta < 1$ (warm colors, magnetically dominated) are underdense due to expansion from magnetic pressure, rise buoyantly, and push out the shock front in two prominent polar lobes.

ties to the magnetic field evolution. Figure 2 demonstrates that the jet experiences significant displacements from the rotation axis of the core in a spiraling motion with helicity opposite to that of the magnetic field (indicated by the magenta colored arrow in Fig. 2), and that the growth rate and dominant instability length scale roughly agree with those predicted by a kink unstable jet in our analysis.

3.2. *Magnetized Expanding Lobes*

Although the initial bipolar jet fails to promptly break out of the stalled shock, MHD becomes dominant tens of milliseconds later. Starting around ∼80 ms after bounce, outflows of highly-magnetized material are continuously launched from the protoneutron star and propagate along the rotation axis of the core. This is depicted in Fig. 3, which presents meridional slices of the plasma parameter β at a range of postbounce times. The highly-magnetized (low-β) high-entropy material does not stay neatly confined to the rotation axis.

In Fig. 4, we present volume renderings of specific entropy and plasma parameter β at 161 ms after bounce. Only these volume renderings speak the full truth about how severely outflows driven by the core are deformed, sheared, and wound up as they propagate in the z-direction. The material that is expelled from the vicinity of the protoneutron star forms tube-like structures that are highly magnetized ($\beta \sim 0.01-0.1$), underdense (∼1% the density of the surrounding fluid), and rise buoyantly. The overall structure of the shocked region evolves toward strongly prolate-shape with two, roughly 90°-filling tilted lobes at both poles (cf. Figs. 1, 3, 4).

The lobes secularly expand to ∼900 km during the simulated time, but their expansion never becomes dynamical. Accreting material is funneled to equatorial regions where it continues to settle onto the protoneutron star. The B-field geometry in the later evolution corresponds to that of a tightly wound coil close to the protoneutron star, but the field lines open up in a spiraling fashion further out, yet still behind the shock. This is consistent with magnetized material moving away from the rotation axis as it propagates in the general z-direction. In 2D simulations, a confining magnetic-tower structure forms instead (Burrows et al. 2007).

4. DISCUSSION

Our results show that 3D magnetorotational core-collapse supernovae are fundamentally different from what has been anticipated on the basis of axisymmetric simulations (Burrows et al. 2007; Dessart et al. 2008; Takiwaki & Kotake 2011). A jet that develops in 2D is disrupted and fizzles in 3D. We suggest that the instability driving this is most likely an MHD kink ($m = 1$) instability to which the toroidally-dominated postbounce magnetic-field configuration is prone. Instead of an axially symmetric jet, a completely new, previously unseen, wide double-lobed flow pattern develops, but we obtain no runaway explosion during the simulated time.

The high precollapse field strength of 10^{12} G yields $\sim 10^{16}$ G in toroidal field and $\beta = P_{\rm gas}/P_{\rm mag} < 1$ within only ∼10−15 ms of bounce, creating conditions favorable for jet formation. Yet, the growth time of the kink instability is shorter than the time it takes for the jet to develop. In a short test simulation with an even more unrealistic, ten times stronger initial field, a successful jet is launched promptly after bounce (consistent with Winteler et al. 2012), but subsequently experiences a spiral instability in its core.

Realistic precollapse iron cores are not expected to have magnetic fields in excess of $\sim 10^8 - 10^9$ G, which may be amplified to no more than $\sim 10^{12}$ G during collapse (Burrows et al. 2007). The $10^{15} - 10^{16}$ G of large-scale toroidal field required to drive a magnetorotational jet must be built up after bounce. This will likely require tens to hundreds of dynamical times, even if the magnetorotational instability operates in conjunction with a dynamo. The results of the present and previous full 3D rotating CCSN simulations (Ott et al. 2007; Kuroda et al. 2013) suggest that MHD and also a variety of nonaxisymmetric hydrodynamic instabilities will grow to non-linear regimes on *shorter timescales*, disrupting any possibly developing axial outflow. *This is why we believe that the dynamics and flow structures seen in our full 3D simulation may be generic to the postbounce evolution of rapidly rotating magnetized core collapse that starts from realistic initial conditions.*

If the polar lobes eventually accelerate, the resulting explosion will be asymmetric, though probably less so than a jet-driven explosion. The lobes carry neutron rich ($Y_e \sim 0.1-0.2$) material of moderate entropy ($s \sim 10-15\,k_B\,{\rm baryon}^{-1}$), which could lead to interesting r-process yields, similar to what Winteler et al. (2012) found for their prompt jet-driven explosion. Even if the lobes continue to move outward, accretion in equatorial regions may continue, eventually (after 2 − 3 s) leading to the collapse of the protoneutron star and black hole formation. In this case, the engine supplying the lobes with low-β plasma is shut off. Unless their material has reached positive total energy, the lobes will fall back onto the black hole, which will subsequently hyperaccrete until material becomes centrifugally supported in an accretion disk. This would set

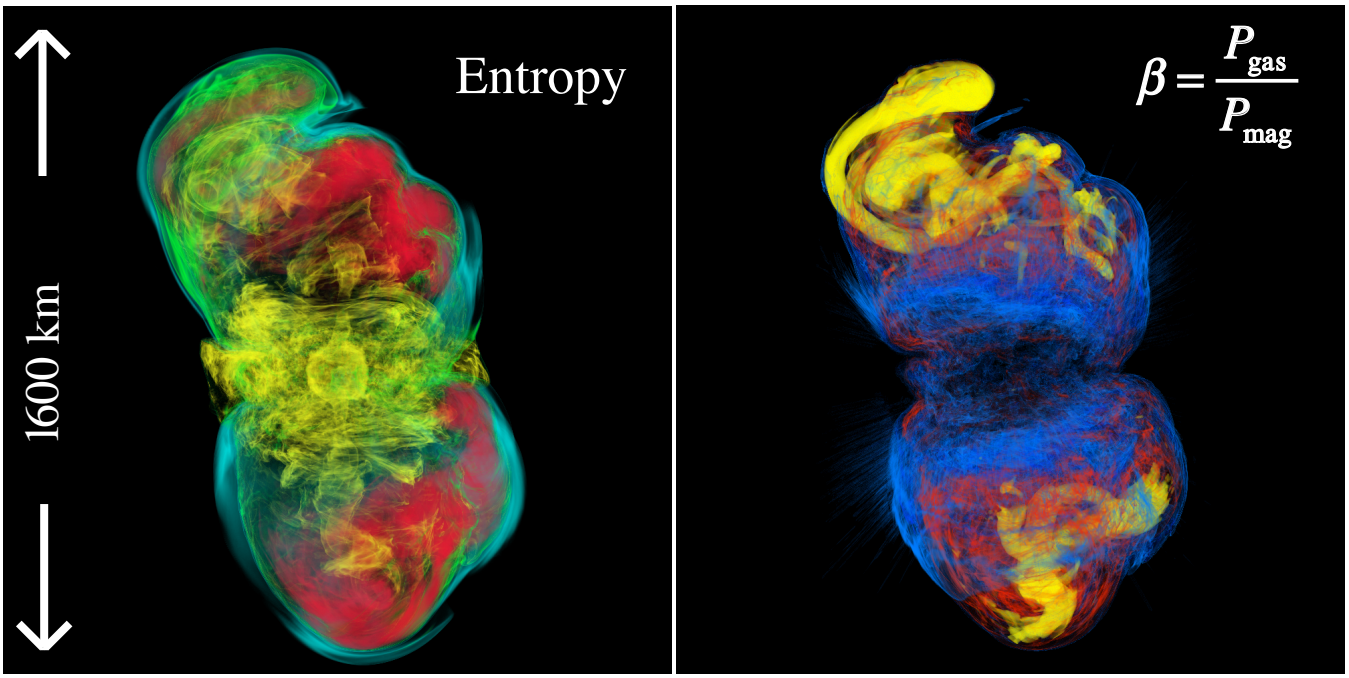

Figure 4. Volume renderings of entropy and β at $t - t_b = 161$ ms. The z-axis is the spin axis of the protoneutron star and we show 1600 km on a side. The colormap for entropy is chosen such that blue corresponds to $s = 3.7 k_b$ baryon^{-1}, cyan to $s = 4.8 k_b$ baryon^{-1} indicating the shock surface, green to $s = 5.8 k_b$ baryon^{-1}, yellow to $s = 7.4 k_b$ baryon^{-1}, and red to higher entropy material at $s = 10 k_b$ baryon^{-1}. For β we choose yellow to correspond to $\beta = 0.1$, red to $\beta = 0.6$, and blue to $\beta = 3.5$. Magnetically dominated material at $\beta < 1$ (yellow) is expelled from the protoneutron star and twisted in highly asymmetric tubes that drive the secular expansion of the polar lobes.

the stage for a subsequent long GRB and an associated Type Ic-bl CCSN that would be driven by a collapsar central engine (Woosley 1993) rather than by a protomagnetar (Metzger et al. 2011).

The results of the present study highlight the importance of studying magnetorotational CCSNe in 3D. Future work will be necessary to explore later postbounce dynamics, the sensitivity to initial conditions and numerical resolution, and possible nucleosynthetic yields. Animations and further details on our simulations are available at http://stellarcollapse.org/cc3dgrmhd.

ACKNOWLEDGMENTS

The authors would like to thank A. Burrows, S. Couch, U. Gamma, D. Meier, and L. Roberts for discussions. This research was partially supported by NSF grants AST-1212170, PHY-1151197, and OCI-0905046, and the Sherman Fairchild Foundation. SR is supported by a DOE Computational Science Graduate Fellowship DE-FG02-97ER25308. CR acknowledges support by NASA through Einstein Fellowship grant PF2-130099. The simulations were carried out on XSEDE (TG-PHY100033) and on NSF/NCSA BlueWaters (PRAC OCI-0941653).

REFERENCES

Akiyama, S., Wheeler, J. C., Meier, D. L., & Lichtenstadt, I. 2003, ApJ, 584, 954
Balbus, S. A., & Hawley, J. F. 1991, ApJ, 376, 214
Begelman, M. C. 1998, ApJ, 493, 291
Bethe, H. A., & Wilson, J. R. 1985, ApJ, 295, 14
Bisnovatyi-Kogan, G. S. 1970, Astron. Zh., 47, 813
Bruenn, S. W., Mezzacappa, A., Hix, W. R., et al. 2013, ApJ, 767, L6
Burrows, A., Dessart, L., Livne, E., Ott, C. D., & Murphy, J. 2007, ApJ, 664, 416
Dessart, L., Burrows, A., Livne, E., & Ott, C. D. 2008, ApJ, 673, L43
Drout, M. R., Soderberg, A. M., Gal-Yam, A., et al. 2011, ApJ, 741, 97
Einfeldt, B. 1988, in Shock tubes and waves; Proceedings of the Sixteenth International Symposium, Aachen, Germany, July 26–31, 1987. VCH Verlag, Weinheim, Germany, 671
Heger, A., Langer, N., & Woosley, S. E. 2000, ApJ, 528, 368
Hjorth, J., & Bloom, J. S. 2011, in Gamma-Ray Bursts, ed. C. Kouveliotou, R. A. M. J. Wijers, & S. E. Woosley (Cambridge, UK: Cambridge University Press)
Kruskal, M., & Tuck, J. L. 1958, Proc. R. Soc. Lond., 245, 222
Kuroda, T., Takiwaki, T., & Kotake, K. 2013, Submitted to Phys. Rev. D., arXiv:1304.4372
Kuroda, T., & Umeda, H. 2010, ApJS, 191, 439
Lattimer, J. M., & Swesty, F. D. 1991, Nucl. Phys. A, 535, 331
LeBlanc, J. M., & Wilson, J. R. 1970, ApJ, 161, 541
Löffler, F., Faber, J., Bentivegna, E., et al. 2012, Class. Quantum Grav., 29, 115001
McKinney, J. C., & Blandford, R. D. 2009, MNRAS, 394, L126
Meier, D. L., Epstein, R. I., Arnett, W. D., & Schramm, D. N. 1976, ApJ, 204, 869
Metzger, B. D., Giannios, D., Thompson, T. A., Bucciantini, N., & Quataert, E. 2011, MNRAS, 413, 2031
Mignone, A., Rossi, P., Bodo, G., Ferrari, A., & Massaglia, S. 2010, MNRAS, 402, 7
Mikami, H., Sato, Y., Matsumoto, T., & Hanawa, T. 2008, ApJ, 683, 357
Modjaz, M. 2011, Astron. Nachr., 332, 434
Mösta, P., Mundim, B. C., Faber, J. A., et al. 2014, Class. Quantum Grav., 31, 015005
Müller, B., Janka, H.-T., & Marek, A. 2012, ApJ, 756, 84
Obergaulinger, M., Cerdá-Durán, P., Müller, E., & Aloy, M. A. 2009, A&A, 498, 241
O'Connor, E., & Ott, C. D. 2010, Class. Quantum Grav., 27, 114103
Ott, C. D., Burrows, A., Thompson, T. A., Livne, E., & Walder, R. 2006, Astrophys. J. Suppl. Ser., 164, 130
Ott, C. D., Dimmelmeier, H., Marek, A., et al. 2007, Phys. Rev. Lett., 98, 261101

Ott, C. D., Abdikamalov, E., O'Connor, E., et al. 2012, Phys. Rev. D, 86, 024026
Reisswig, C., Haas, R., Ott, C. D., et al. 2013, Phys. Rev. D, 87, 064023
Scheidegger, S., Käppeli, R., Whitehouse, S. C., Fischer, T., & Liebendörfer, M. 2010, A&A, 514, A51
Shafranov, V. 1956, At. Energy, 5, 38
Shibata, M., Liu, Y. T., Shapiro, S. L., & Stephens, B. C. 2006, Phys. Rev. D, 74, 104026
Soderberg, A. M., Kulkarni, S. R., Nakar, E., et al. 2006, Nature, 442, 1014
Takiwaki, T., & Kotake, K. 2011, ApJ, 743, 30
Tchekhovskoy, A., McKinney, J. C., & Narayan, R. 2007, Mon. Not. Roy. Astron. Soc., 379, 469
Thompson, T. A., Quataert, E., & Burrows, A. 2005, ApJ, 620, 861
Tóth, G. 2000, J. Comp. Phys., 161, 605
Wheeler, J. C., Meier, D. L., & Wilson, J. R. 2002, ApJ, 568, 807
Winteler, C., Käppeli, R., Perego, A., et al. 2012, ApJ, 750, L22
Woosley, S. E. 1993, ApJ, 405, 273